Available online at www.sciencedirect.com
SCIENCE DIRECT®
Journal of Magnetic Resonance 161 (2003) 25–34
JMR Journal of Magnetic Resonance
www.elsevier.com/locate/jmr

Multi-exponential analysis of magnitude MR images using a quantitative multispectral edge-preserving filter

Jean-Marie Bonny,[a,*] Odile Boespflug-Tanguly,[b] Michel Zanca,[c] and Jean-Pierre Renou[a]

[a] *INRA Unité STIM, Centre de Theix, 63122 Saint-Genès Champanelle, France*
[b] *INSERM Unité 384, Faculté de Médecine, 63001 Clermont-Fd, France*
[c] *MIR Biophysique et Médecine Nucléaire, CMC Gui-de-Chauliac, 2 avenue Bertin-Sans, 34295 Montpellier Cedex 5, France*

Received 24 June 2002; revised 11 October 2002

Abstract

A solution for discrete multi-exponential analysis of T_2 relaxation decay curves obtained in current multi-echo imaging protocol conditions is described. We propose a preprocessing step to improve the signal-to-noise ratio and thus lower the signal-to-noise ratio threshold from which a high percentage of true multi-exponential detection is detected. It consists of a multispectral nonlinear edge-preserving filter that takes into account the signal-dependent Rician distribution of noise affecting magnitude MR images. Discrete multi-exponential decomposition, which requires no a priori knowledge, is performed by a non-linear least-squares procedure initialized with estimates obtained from a total least-squares linear prediction algorithm. This approach was validated and optimized experimentally on simulated data sets of normal human brains.

Keywords: Quantitative MRI; Multispectral filter; Multi-exponential analysis; T_2 relaxation; Linear prediction

1. Introduction

Multi-exponential fitting techniques are important for a realistic analysis of T_2 relaxation curves measured in biological tissues. This is especially true for the in vivo study of human brain white matter (WM) [1].

Multi-exponential decomposition is an example of a linear inverse problem with discrete data. It affords dependent solutions because the projection basis, composed by the different exponential functions, is severely non-orthogonal. This kind of inverse problem is ill-posed [2]: a small error in the data (the main result of noise) can produce an extremely large error in the solutions, which may therefore lose all physical meaning.

Owing to the intrinsic trade-off between signal-to-noise ratio (SNR) and spatial resolution, and the necessarily limited acquisition time available for in vivo studies, the current multi-echo imaging protocol leads to limited SNR (≈ 100). Also, the minimum interval between successive samples, ΔTE, cannot be less than 10 ms. Multi-exponential analysis is thus challenging, especially when two relaxation components are to be resolved from a limited number N of points that rapidly approach noise levels. Because of these technical restrictions of MRI, only a few implementations have been described for the characterization of tissues [3–12] or pathology [13–15].

Here, a general two-step approach is proposed for performing a multi-exponential decomposition from multi-echo images obtained in limited SNR and ΔTE conditions. The first step uses a multispectral non-linear edge-preserving (MNLEP) filter [16], modified to account for the Rician nature of the magnitude data. The second step is a discrete multi-exponential decomposition performed by a non-linear least-squares (NLLS) fitting procedure initialized with parameter guesses obtained from a total least-squares linear prediction (LPTLS) procedure.

This approach was tested and validated on simulated datasets characterized by the multi-exponential behavior of normal human brains. Potential practical applications

* Corresponding author. Fax: +33-4-73-62-45-21.
E-mail address: bonny@clermont.inra.fr (J.-M. Bonny).

1090-7807/03/$ - see front matter © 2003 Elsevier Science (USA). All rights reserved.
doi:10.1016/S1090-7807(02)00107-6

of this multi-exponential reconstruction method are proposed.

2. Theory

Several studies have demonstrated from Monte-Carlo simulations that SNR must exceed a critical threshold for a two-component T_2 distribution to be resolved [17–19]. In the example of bi-exponential T_2 relaxation (long-T_2 component of 80 ms and short-T_2 component of 20 ms with a relative amplitude of 15%) and the sampling conditions ($TE_1 = 20$ ms, $\Delta TE = 15$ ms), the SNR must exceed a threshold of 1000 to guarantee that the *Cramér-Rao* lower bound (CRLB) is less than 10% for each parameter, and insure tolerable accuracy in the estimation of the shortest relaxation time.

Spatial filtering offers a way to improve SNR while obviating increased acquisition time, which is unacceptable for in vivo studies. An appropriate filter should meet the following criteria:

1. It should preserve the edge information (object boundaries) so that no additional partial volume effect is introduced.
2. It should take into account the Rician behavior of noisy magnitude signals for the estimation of the underlying true intensity. This is especially important in the case of multi-exponential decomposition, since late-TE images are characterized by regions displaying poor SNR, producing severe discrepancies between observed magnitude and true intensity [20,21].
3. It should use interframe information, since a multispectral signal (i.e., vector-valued, multichannel or multivariate) of size N is available in each voxel location. This property insures that all echo images are processed simultaneously.

To meet these conditions, the main principles of the multispectral nonlinear edge-preserving (MNLEP) filter introduced by Soltanian-Zadeh et al. [16] were adopted. The original algorithm was modified to incorporate the Rician probability distribution of magnitudes. Let W be a window of finite size S. If M_i^j is the magnitude of frame j (i.e., the image obtained at TE_j, in our multi-echo protocol) observed in the ith voxel of the window W centered on the processed voxel with $1 \leqslant i \leqslant S$, the vector-valued magnitude signal is $\mathbf{M}_i = [M_i^1, M_i^2, \ldots, M_i^N]^T$. The first step of the MNLEP filter is a discrimination stage which consists in using the interframe information to select the voxels of W representing the same tissue. Hence the Euclidean distance between the ith voxel vector of W and the voxel vector in the center of W is calculated and compared with a user-defined threshold η. This ith voxel vector is considered to represent the same tissue as the central voxel vector if the distance is smaller than the threshold η. By repeating this comparison for each voxel of W, the Euclidean distance discriminator gathers a set $\{\mathbf{M}_1, \mathbf{M}_2, \ldots, \mathbf{M}_K\}$ of K magnitude vectors $1 \leqslant K \leqslant S$ that are considered to represent the same tissue and thus differ only by noise, assuming spatial ergodicity. The second step of the MNLEP filter consists in attributing a de-noised signal to the central voxel estimated from the K observations (intraframe smoothing). The amplitude $\hat{M}^j$ of frame j attributed to the central voxel is given by

$$\hat{M}^j = \mathbf{F}(M_1^j, M_2^j, \ldots, M_K^j), \tag{1}$$

where $\mathbf{F}$ is any scheme that gives an estimate of the true intensity from noisy magnitude samples (see appendix A). This estimation step is applied for each frame j and then repeated N times.

The final algorithm implemented for multi-exponential analysis of T_2 decay curves successively uses this MNLEP filter adapted to magnitude images, and a discrete multi-exponential decomposition (see above).

3. Materials and methods

3.1. Multi-exponential decomposition

In the case of discrete sums of P exponentials and Gaussian distributed samples, the nonlinear least-squares (NLLS) method is well-suited for performing multi-exponential analysis in a statistically optimal way. NLLS finds the set of parameters that minimizes the following least-squares χ^2 misfit

$$\chi^2(P) = \frac{1}{\sigma_F^2} \sum_{i=1}^{N} \left[\hat{M}^i - \sum_{j=1}^{P} A_j \exp\left(-\frac{TE_i}{T_j} \right) \right]^2, \tag{2}$$

where T_j and A_j refer respectively to the relaxation time and the amplitude for the jth exponential component, and σ_F the standard deviation of noise after filtering. The NLLS method has two major prerequisites: the number P of exponentials must be known, and a set of good enough initial parameter guesses has to be provided.

For that purpose, an operator-independent inversion algorithm based on the linear prediction (LP) principle was used, which requires no parameter guesses. The LP model of *Prony* was also used to fit a finite number of exponentially damped sinusoids to the time-domain NMR signal [22]. It is applicable to the multi-exponential decays under the constraint that all sinusoid phases and frequencies are equal and null. The linear prediction problem is solved in the total least-squares (TLS) sense to produce accurate estimates of the remaining damping factors, in spite of low SNR decays [23,24].

To decide the number P of exponentials, multi-exponential analysis was applied iteratively with increasing values of P until no additional exponential could be considered as further improving the χ^2 misfit. For this purpose, an F test was used [25]. An additional expo-

nential component was judged to improve fit only if the probability that the noise accounted for the i misfit improvement when comparing $\chi^2(P)$ and $\chi^2(P+1)$ was under 1%.

3.2. Analysis of the quantitative impact of filtering prior to multi-exponential analysis

The algorithm was validated on simulated data sets because it defines a ground truth for a given SNR in contrast to in vivo acquisition. The quantitative impact of MNLEP preprocessing on homogeneous noisy regions was first studied (i.e., noise filtration). For this purpose, 1000 Rician-distributed bi-exponential relaxation curves of size $K = 5 \times 5$ were simulated (32 echo times with $\mathrm{TE}_1 = \Delta\mathrm{TE} = 10\,\mathrm{ms}$). For each frame at a given TE, the true amplitude $a(\mathrm{TE})$ was estimated using three different estimators: the arithmetic mean, the bias corrected quadratic mean and the maximum likelihood estimator. Each of these is described in the appendix. Finally the multi-exponential analysis was applied and the performance of the different estimators was compared for the percentage of bi-exponential detection and the bias and standard deviation of the estimated parameters (i.e., the short and long relaxation times T_S and T_L and the relative amplitude A_S of the short component). This comparison was made in two different situations, for varying SNR and constant tissue characteristics (corresponding to the WM model of Table 1), and for constant SNR ($=100$) and varying relative amplitude of T_s (see Fig. 1).

Noisy Rician-distributed magnitudes were generated by taking the magnitudes of real and imaginary signals obtained by adding two independent Gaussian noises to the true values $a(\mathrm{TE}) \cdot \cos\phi$ and $a(\mathrm{TE}) \cdot \sin\phi$, where ϕ is a constant phase value. Gaussian noises were generated using the random_normal subroutine of the mathematical IMSL library (Visual Numerics, Houston, TX), and the level of noise σ was adjusted by defining SNR as

$$\mathrm{SNR} = a(\mathrm{TE}=0)/\sigma = \sigma^{-1}. \tag{3}$$

3.3. Analysis of edge preservation

Synthetic multi-echo images were derived from the anatomical model of normal human brain developed at the McConnell Brain Imaging Center (http://www.bic.mni.mcgill.ca/brainweb/) [26]. This model consisted of a set of tissue membership volumes, one for each tissue class. The voxel value reflected the proportion of tissue present in that voxel. 2D simulated multi-echo images composed of 32 frames at different echo times ($\mathrm{TE}_1 = \Delta\mathrm{TE} = 10\,\mathrm{ms}$) were generated from the three main tissue classes of the model (CSF, WM, and GM). In each voxel, the true intensity a of each frame displayed the following multi-exponential behavior

$$a(\mathrm{TE}) = v_{\mathrm{CSF}} \cdot a_{\mathrm{CSF}}(\mathrm{TE}) + v_{\mathrm{GM}} \cdot a_{\mathrm{GM}}(\mathrm{TE}) + v_{\mathrm{WM}} \cdot a_{\mathrm{WM}}(\mathrm{TE})$$

with

$$v_{\mathrm{CSF}} + v_{\mathrm{GM}} + v_{\mathrm{WM}} = 1, \tag{4}$$

where a_i and v_i represent respectively the T_2 decay curve and the proportion for the tissue class i. The parameters characterizing the behavior of the T_2 decay curve a_i for each considered tissue class are indicated in Table 1.

In the MNLEP scheme, the Euclidean distance between a voxel vector in the moving window W and the voxel vector in the center is calculated and compared with a specific threshold η [16]. Thus η results from a trade-off between suppression of noise and preservation of original partial volume effect. To solve this problem, the mean absolute difference (MAD) was calculated for different values of η. This index defined by

$$\mathrm{MAD} = \sum_{\mathbf{r}}^{\mathrm{Image}} |p_\eta(\mathbf{r}) - p(\mathbf{r})| \tag{5}$$

measures the global error between the map of parameter p_η obtained with the threshold η in the MNLEP-Quadratic filter (i.e., the MNLEP version integrating the bias-corrected quadratic mean, $S = 5 \times 5$) and the reference map of the parameter p obtained by multi-exponential decomposition of noise-free images. This sum was calculated for each parameter, normalized and presented in Fig. 2.

Finally, the edge preservation properties of MNLEP-Quadratic filter ($\eta = 3$, $S = 5 \times 5$) were studied and compared with those of alternative filters; the Gaussian linear filter and the vector median non-linear filter. The width of the Gaussian impulse response was adjusted to induce approximately the same level of noise reduction as the MNLEP filter. The vector median approach ($S = 5 \times 5$) was chosen because it concerns an edge-preserving multispectral filter, which performs best performance for noise attenuation compared with the other multispectral filters based on the reduced ordering principle [27]. Fig. 3 shows profiles obtained by applying these different filters prior to multi-exponential analysis.

Data were processed on an IRIX O2 workstation (Silicon Graphics, Mountain View, CA). The software, including filtering, multi-exponential analysis, numerical

Table 1
Parameters characterizing the behavior of the T_2 decay curve for the three tissue classes considered in the simulation

Tissue type	Number of components	Relaxation time (ms)	Amplitude
CSF	1	2000	1.0
GM	1	100	1.0
		80	0.90
WM	2	20	0.10

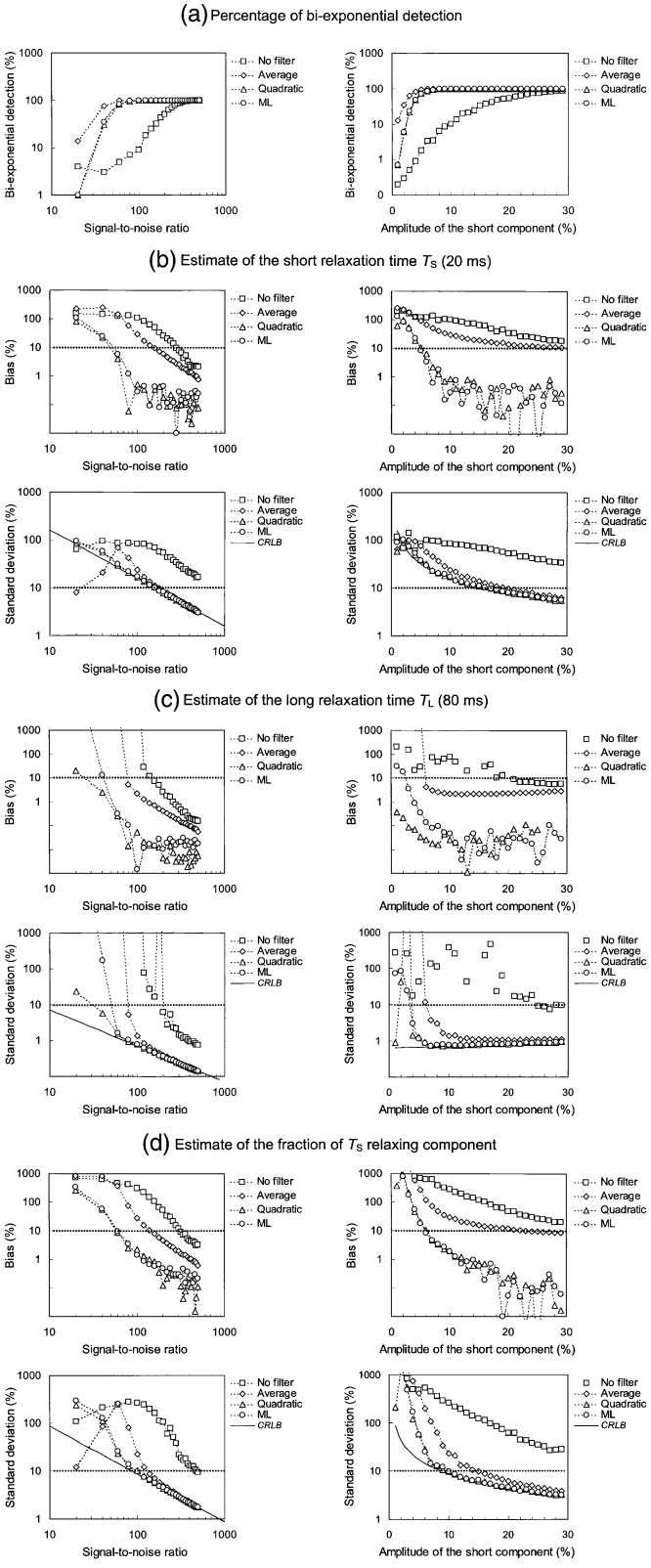

Fig. 1. Performance of bi-exponential analysis for different estimators of the true magnitude as a function of the signal-to-noise ratio (left side) and as function of the relative amplitude A_S of the short relaxing component (right side). The estimators were the arithmetic mean (average), the bias-corrected quadratic mean (quadratic) and the maximum likelihood scheme (ML). The dotted lines indicate a threshold of 10%, bias or standard deviations above this level correspond arbitrarily to an intolerable degradation of accuracy.

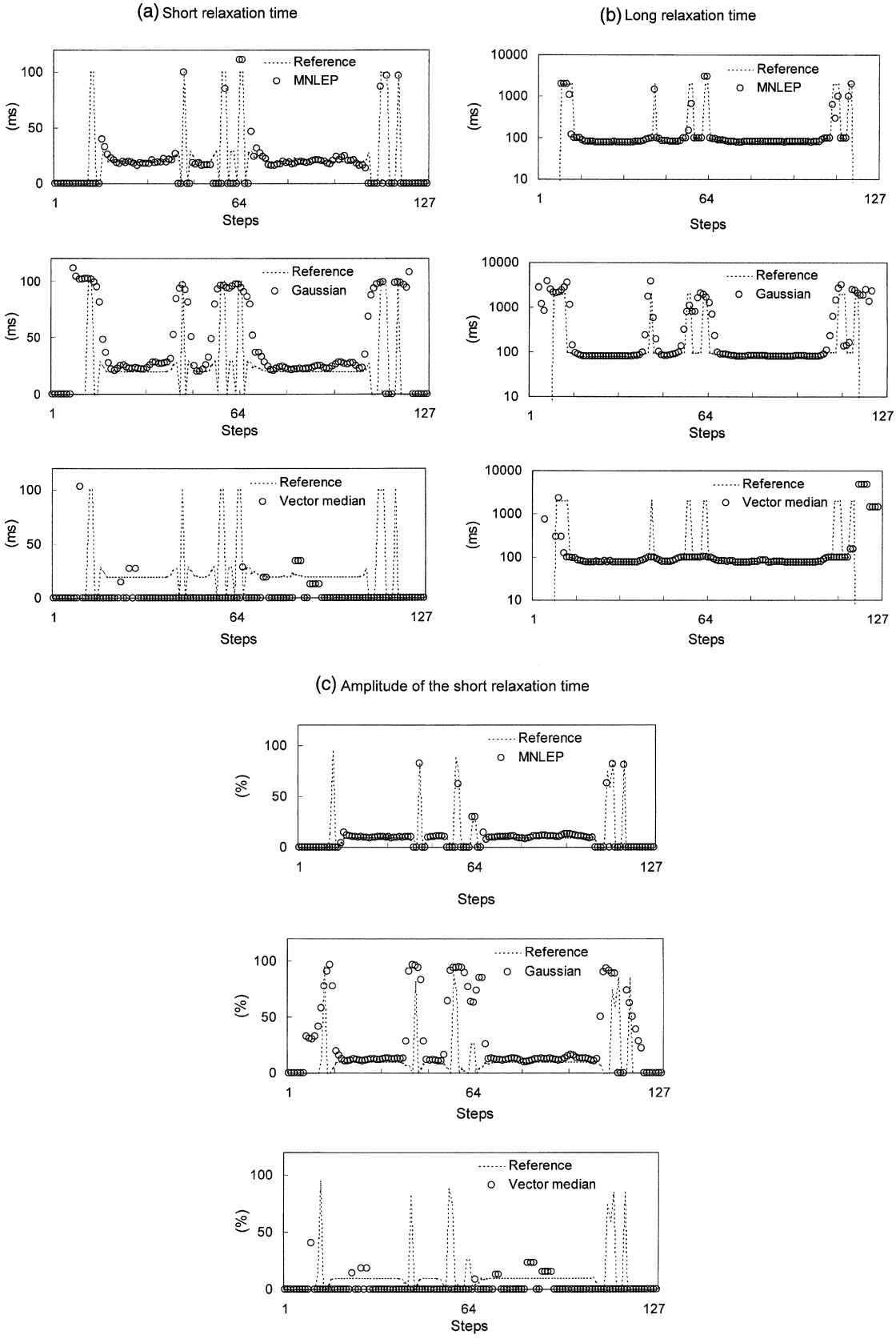

Fig. 2. Mean absolute difference using different values of threshold η in the MNLEP-Quadratic filter ($S = 5 \times 5$).

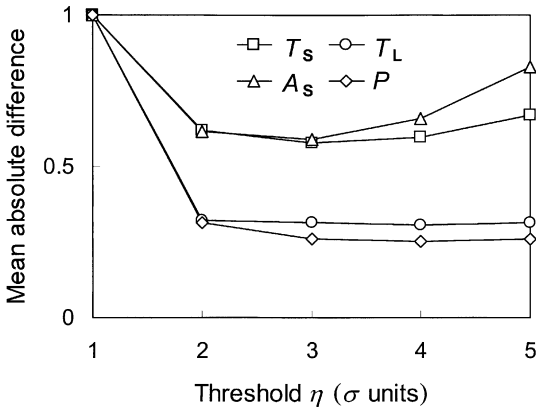

Fig. 3. Profiles measured in the multi-exponential maps using different filters prior to multi-exponential analysis; the MNLEP-Quadratic filter ($S = 5 \times 5$, $\eta = 3\sigma$), the Gaussian linear filter (impulse response width of 1.41 leading to a noise reduction factor of 5) and the vector median before ($S = 5 \times 5$). The chosen profile is a horizontal line passing through the splenium of the corpus callosum of Fig. 4.

simulations and image visualization, was developed by us using mathematical IMSL and ImageVision libraries

4. Results

4.1. Quantitative impact of filtering prior to multi-exponential analysis

The basic result obtained from the Fig. 1 is that a regularization step prior to multi-exponential analysis improves the percentage of bi-exponential detection and decreases both bias and uncertainties in the estimated parameters. More precisely, the MNLEP filtering markedly improves the detection of true bi-exponential behavior for a wide range of SNR and amplitude of the short component. For varying SNR and without filtering (see left side of Fig. 1(a)), the curve behaves as a sigmoid characterized by a continuous decrease in performance for SNRs ranging from 100 to 300. With filtering, the percentage of detection is optimal for SNR above 100, with a rapid drop in performance below a critical threshold SNR of ≈50–100. The ability to detect a short component of variable amplitude is also improved when filtering is applied (see right side of Fig. 1(a)). Moreover, this ability does not depend on the value of the amplitude itself, contrary to what is observed when no filter is applied. Figs. 1(b)–(d) shows that the lowest bias and uncertainties in the estimated parameters were always obtained using the bias-corrected quadratic mean and the maximum likelihood estimator, supporting their superiority in taking into account the Rician-distributed data sets. The lowest accuracy was obtained on T_S, which is explained by the lowest CRLB indicating the lowest expected bias-variance trade-off among all the parameters. These results also support the choice of the bias-corrected quadratic mean instead of maximum likelihood estimator in the MNLEP filter because their performance is almost equivalent for moderate size $S(\approx 5 \times 5)$ of window, and because the bias-corrected quadratic mean requires less computation.

In the case of mono-exponential behavior of decay curves (results not shown), the MNLEP step slightly improves the uncertainties in the estimated parameters and introduces only a few further partial volume effects, false bi-exponential behavior seldom being detected.

4.2. Edge preservation

For the parameters T_L and P, the MAD index shown in Fig. 2 is almost constant and minimum for $\eta \geqslant 3\sigma$. For both T_S and A_S, an optimal threshold is observed for $\eta = 3\sigma$. Hence the mutual minimum 3σ should be selected for η as an efficient trade-off between smoothing and limitation of additional partial volume effect.

Fig. 3 clearly demonstrates the ability of the multi-exponential decomposition method integrating the MNLEP-Quadratic filter ($\eta = 3$, $S = 5 \times 5$) to generate profiles with small bias and low partial volume effect. In comparison, while Gaussian linear filter is efficient for noise smoothing and so for detecting bi-exponential behavior, it introduces severe artifacts due mainly to the partial volume effect near the transitions between regions. Conversely, the vector median filter does not introduce any further partial volume effect, but the noise reduction factor is too low to detect the multi-exponential processes. The detected single component is thus mainly influenced by the bulk component of the noisy multi-exponential process. These results are explained by the properties of median filters, which are designed to filter signals contaminated by long-tailed distributed noise (e.g., impulsive noise), which is not the case for the Rician-distributed noise.

Fig. 4 compares the different maps obtained using the MNLEP-Quadratic filter ($\eta = 3$, $S = 5 \times 5$) or no filter at all with the ground truth for SNR = 100. Visually, the main improvement concerns the better detection of the short component T_S in WM owing to the lower impact of propagated noise when the modified MNLEP filter is applied. Moreover, the edges are well preserved near the transitions between the different tissues, for example near the boundaries between WM and GM. Problems occur for voxels showing partial volume effects between GM and CSF. In this case, the results depend on their relative amplitudes. Best results are obtained for approximately equal populations (fraction ≈ 40–60%). If a single exponential is detected, the remaining relaxation time ranges between T_S and T_L but is only loosely related to the weighted mean (i.e., $A_S T_S + (1 - A_s) T_L$).

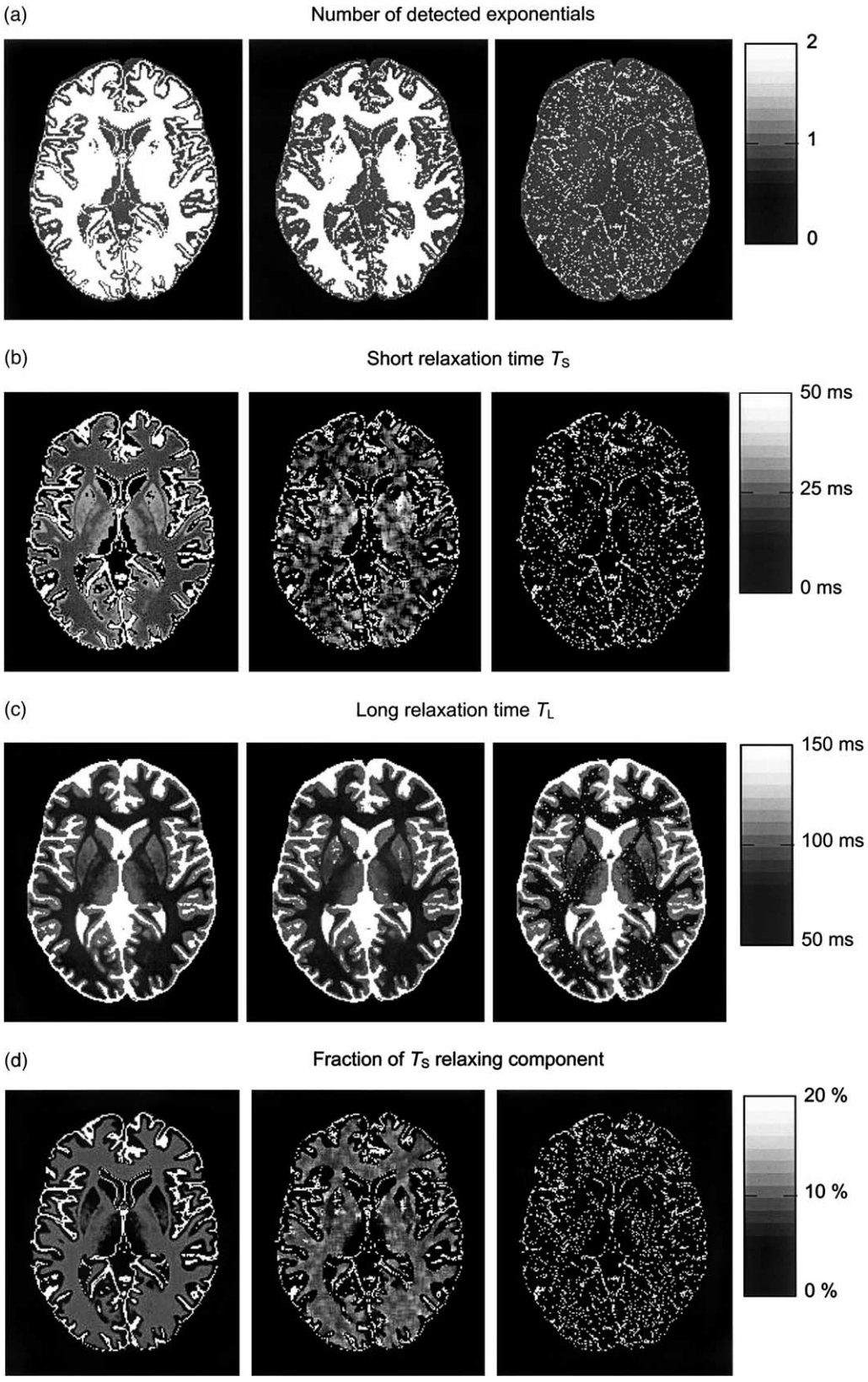

Fig. 4. Multi-exponential maps obtained from noise-free multi-echo images (left side), from noisy multi-echo images filtered by a MNLEP-Quadratic scheme ($S = 5 \times 5$, $\eta = 3\sigma$) before multi-exponential analysis (center) and from noisy multi-echo images with no filter (right side). In this bi-exponential situation at SNR = 100, four different maps are reconstructed: (a) indicating the number P of detected exponentials (i.e., one or two), (b) giving the short exponential component T_S, (c) giving the long exponential components T_L and (d) corresponding to the relative fraction of T_S. When only one exponential component is resolved, the value is arbitrarily attributed to the T_L-map and the value of T_S is set to zero.

5. Discussion

An elevated SNR is essential for detecting bi-exponential behavior of relaxation curves in experimental conditions. The results presented here, obtained on simulated decay curves and images, show that a pre-processing step with the modified MNLEP filter improves the multi-exponential analysis. For both varying SNR and amplitude of the short component, the percentage of bi-exponential detection increases (see Fig. 1(a)), while both bias and uncertainty are significantly reduced (see Figs. 1(b)–(d)). The effects of Rician noise were better corrected using the bias-corrected quadratic mean or the maximum-likelihood estimator. It is important to stress that the non-zero mean of magnitude in the region of low SNR should not be interpreted as a constant offset, and thus that the latter estimation schemes should not be replaced by a subtraction of a constant offset from the entire decay curve.

Alternative filtering approaches have recently been proposed to meet the first two conditions stated above (i.e., edge preservation and consideration of Rician behavior of noise), namely a wavelet-based scheme applied on either the square magnitude image [28] or the two channels of the complex image [29,30], and an anisotropic diffusion filter [31]. Though efficient, these filters addressed the case of a single image and so do not meet the third condition (i.e., the use of multispectral information). Conversely, a multispectral form of anisotropic diffusion filter has been proposed [32] that does not address the Rician behavior of noise.

Whatever the estimation scheme chosen, the MNLEP filter requires an estimate $\hat{\sigma}$ of the a priori unknown noise standard deviation σ (see Eqs. A.3 and A.5). In practice, a large region of interest was manually placed in the magnitude image background, and $\hat{\sigma}$ was calculated from the selected values [33]. Hence $\hat{\sigma}$ is not perfectly error-free, owing to the possible presence of ringing, motion and/or ghosting artifacts in the region of interest. Simulations indicate that a large error in $\hat{\sigma}$ is tolerable, because when an error of σ was introduced in the MNLEP filter, bi-exponential behavior was still detected for the whole set of voxels. A large 10% under- (or over-) estimation of σ produced a positive (or negative) bias on the estimated parameters. Underestimation of σ also produced a significant increase in uncertainties.

Since the LP procedure is used for multi-exponential decomposition, the value of prediction order L has to be chosen a priori. It is generally advised to choose the LP matrix as square as possible, i.e., $L \approx N/2$ [34]. We performed multi-exponential decompositions with different values of L, which indicated that the LPTLS algorithm will tolerate a wide range of values for the prediction order (especially when SNR increases) provided it is chosen larger than the number P of exponentials. In practice, a constant value $L = (N-1)/2$ was chosen. In this case the LPTLS method finds the single solution to an over-determined linear prediction problem. The proposed algorithm based on an NLLS procedure initialized with estimates obtained from an LPTLS algorithm was chosen because it directly produces a discrete decomposition of decay curves, which can be displayed in the form of parametric maps. This circumvents the integration necessary to go from a regularized decomposition in a continuum of relaxation constants [10] to a non-continuous set of relaxing components. However, it is possible to use a continuous decomposition method (e.g., non-negative least squares algorithm) instead of the present discrete one for characterizing components that are poorly modeled by a delta function, and to benefit from the SNR boost due to MNLEP filtering.

The multi-exponential method is applicable to any type of decay data obtained by MR imaging, such as *T2*-decay or diffusion-weighted decay obtained with increasing *b*-factor [35]. However, LP exclusively handles evenly sampled data, i.e., $\mathrm{TE}_i = \mathrm{TE}_0 + i \cdot \Delta\mathrm{TE}$. In the case of uneven sampling, the decay must be interpolated voxelwise prior to multi-exponential decomposition.

We first demonstrate that the MNLEP filter, modified to take into account the Rician behavior of noisy magnitude signals, is a general solution to improve the SNR of MR images before parameter estimation, with no increase in acquisition time. Moreover, the LPTLS algorithm followed by the NLLS scheme and validated by an F test is an efficient approach for obtaining discrete multi-exponential decomposition, without introduction of a priori knowledge.

Acknowledgments

We thank Dr. K.P. Whittall for carefully reading the first manuscript and for helpful comments.

Appendix A

After interframe discrimination step which is the first step of a MNLEP filter [16], a Rician-distributed data set of K noisy magnitudes is available from which the true amplitude must be estimated, i.e.,

$$\hat{M}_{\mathrm{F}} = \mathbf{F}(M_1, M_2, \ldots, M_K). \tag{A.1}$$

Note that the superscript corresponding to the frame index has been discarded (see Eq. (1)), because the same estimation step is applied for each of the N frames. To a specific estimator corresponds a version of MNLEP filter differing from their noise regularization properties. The simplest estimator $\mathbf{F}$ is the following arithmetic mean

$$\hat{M}_{\text{Mean}} = \frac{1}{K}\sum_{i=1}^{K} M_i. \quad \text{(A.2)}$$

It is well-known that $\hat{M}_{\text{Mean}}$ is the maximum likelihood (ML) optimal estimator for Gaussian distributed samples. Hence it becomes biased as SNR decreases due to marked deviation of the Rician distribution compared with the Gaussian one [21,36]. It is not possible to remove the bias affecting $\hat{M}_{\text{Mean}}$ by simply subtracting a constant baseline because the bias depends on the SNR. An alternative consists in employing the unbiased estimator $\hat{M}_{\text{Quadratic}}$ of the underlying signal based on the quadratic mean given by [37,38]

$$\lambda = \frac{1}{K}\sum_{i=1}^{K} M_i^2 - 2\sigma^2 \quad \text{(A.3)}$$

$$\text{if } \lambda \geqslant 0 \text{ then } \hat{M}_{\text{Quadratic}} = \sqrt{\lambda} \text{ else } \hat{M}_{\text{Quadratic}} = 0, \quad \text{(A.4)}$$

where σ is the standard deviation of the zero-mean Gaussian noise affecting the real and imaginary images.

Though unbiased, this estimator is theoretically suboptimal [21,39]. On the contrary, the ML approach is optimal because as the number of samples increases the bias tends to zero and the covariance matrix of the estimates converges towards the *Cramér-Rao* bound. ML estimation of the true amplitude is obtained by finding the maximum of the log-likelihood function of the samples. This is done by solving the following non-linear equation (i.e., the stationary condition of the log-likelihood function) which was first introduced in [33]:

$$\hat{M}_{\text{ML}} - \frac{1}{K}\sum_{i=1}^{K} M_i \frac{I_1}{I_0}\left(\frac{M_i \hat{M}_{\text{ML}}}{\sigma^2}\right) = 0, \quad \text{(A.5)}$$

where I_1 is the first-order modified Bessel function, the first derivative of I_0. If (A.3) is strictly positive, Eq. (A.5) leads to three solutions; 0 and two symmetric solutions $\pm\beta$ with $\beta > 0$ [39]. In practice, only β is relevant. To select this root, a practical solution consists in solving Eq. (A.5) using any iterative mono-dimensional root finding method initialized by the estimate $\hat{M}_{\text{Quadratic}}$ given by Eq. (A.4). If (A.3) is not strictly positive, that may be possible for particular realizations of the noise, the single solution is $\hat{M}_{\text{ML}} = 0$ [39].

References

[1] K.P. Whittall, A.L. MacKay, D.K. Li, Are mono-exponential fits to a few echoes sufficient to determine T2 relaxation for in vivo human brain? Magn. Reson. Med. 41 (1999) 1255–1257.

[2] M. Bertero, C. DeMol, E.R. Pike, Linear inverse problems with discrete data. I: General formulation and singular system analysis, Inverse Problems 1 (1985) 301–330.

[3] K. Gersonde, L. Felsberg, T. Tolxdorff, D. Ratzel, B. Strobel, Analysis of multiple T2 proton relaxation processes in human head and imaging on the basis of selective and assigned T2 values, Magn. Reson. Med. 1 (1984) 463–477.

[4] M.D. Does, J.C. Gore, Rapid acquisition transverse relaxometric imaging, J. Magn. Reson. 147 (2000) 116–120.

[5] R.L. Kamman, C.J. Bakker, P. van Dijk, G.P. Stomp, A.P. Heiner, H.J. Berendsen, Multi-exponential relaxation analysis with MR imaging and NMR spectroscopy using fat-water systems, Magn. Reson. Imaging 5 (1987) 381–392.

[6] A. Fransson, A. Ericsson, B. Jung, U. Henriksson, Resolution of biexponential transverse relaxation in magnetic resonance imaging, Phys. Med. Biol. 34 (1989) 305–314.

[7] R.V. Mulkern, S.T. Wong, P. Jakab, A.R. Bleier, T. Sandor, F.A. Jolesz, CPMG imaging sequences for high field in vivo transverse relaxation studies, Magn. Reson. Med. 16 (1990) 67–79.

[8] K.H. Cheng, In vivo tissue characterization of human brain by chisquares parameter maps: multiparameter proton T2-relaxation analysis, Magn. Reson. Imaging 12 (1994) 1099–1109.

[9] A. MacKay, K. Whittall, J. Adler, D. Li, D. Paty, D. Graeb, In vivo visualization of myelin water in brain by magnetic resonance, Magn. Reson. Med. 31 (1994) 673–677.

[10] K.P. Whittall, A.L. MacKay, D.A. Graeb, R.A. Nugent, O.K. Li, D.W. Paty, In vivo measurement of T2 distributions and water contents in normal human brain, Magn. Reson. Med. 37 (1997) 34–43.

[11] P.J. Gareau, B.K. Rutt, C.V. Bowen, S.J. Karlik, J.R. Mitchell, In vivo measurements of multi-component T2 relaxation behaviour in guinea pig brain, Magn. Reson. Imaging 17 (1999) 1319–1325.

[12] M.D. Does, R.E. Snyder, Multiexponential T2 relaxation in degenerating peripheral nerve, Magn. Reson. Med. 35 (1996) 207–213.

[13] L.R. Schad, G. Brix, W. Semmler, F. Guckel, W.J. Lorenz, Two-exponential analysis of spin-spin proton relaxation times in MR imaging using surface coils, Magn. Reson. Imaging 7 (1989) 357–362.

[14] L.R. Schad, G. Brix, I. Zuna, W. Harle, W.J. Lorenz, W. Semmler, Multiexponential proton spin-spin relaxation in MR imaging of human brain tumors, J. Comput. Assist. Tomogr. 13 (1989) 577–587.

[15] J.P. Armspach, D. Gounot, L. Rumbach, J. Chambron, In vivo determination of multiexponential T2 relaxation in the brain of patients with multiple sclerosis, Magn. Reson. Imaging 9 (1991) 107–113.

[16] H. Soltanian-Zadeh, J.P. Windham, A.E. Yagle, A multidimensional nonlinear edge-preserving filter for magnetic resonance image restoration, IEEE Trans. Image Process. 4 (1995) 147–161.

[17] K.P. Whittall, MJ. Bronskill, and R.M. Henkelman, Investigation of analysis techniques for complicated NMR relaxation data, J. Magn. Reson. 95 (1991) 221–234.

[18] N.J. Clayden, B.D. Hesler, Multiexponential analysis of relaxation decays, J. Magn. Reson. 98 (1992) 271–282.

[19] S.J. Graham, P.L. Stanchev, M.J. Bronskill, Criteria for analysis of multicomponent tissue T2 relaxation data, Magn. Reson. Med. 35 (1996) 370–383.

[20] R.M. Henkelman, Measurement of signal intensities in the presence of noise in MR images, Med. Phys. 12 (1985) 232–233.

[21] H. Gudbjartsson, S. Patz, The Rician distribution of noisy MRI data [published erratum appears in Magn Reson Med 1996 Aug;36(2):332], Magn. Reson. Med. 34 (1995) 910–914.

[22] H. Barkhuijsen, R. De Beer, M.M. Bovée, D. Van Ormondt, Retrieval of frequencies amplitudes damping factors and phases from time-domain signals using a linear least-squares procedure, J. Magn. Reson. 61 (1985) 465–481.

[23] A. Rahman, K.B. Yu, Total least squares approach for frequency estimation using linear prediction, IEEE Trans. Acoustics Speech Signal Process. ASSP-35 (1987) 1440–1454.

[24] C.F. Tirendi, J.F. Martin, Quantitative analysis of NMR spectra by linear prediction and total least squares, J. Magn. Reson. 85 (1989) 162–169.
[25] B.E. Dumitresco, J.P. Armspach, D. Gounot, D. Grucker, Y. Mauss, J. Steibel, D. Wecker, J. Chambron, Multi-exponential analysis of T2 images, Magn. Reson. Imaging 4 (1986) 445–448.
[26] R.K. Kwan, A.C. Evans, G.B. Pike, MRI simulation-based evaluation of image-processing and classification methods, IEEE Trans. Med. Imaging 18 (1999) 1085–1097.
[27] K. Tang, J. Astola, Y. Neuvo, Nonlinear multivariate image filtering techniques, IEEE Trans. Image Process. 4 (1995) 788–798.
[28] R.D. Nowak, Wavelet-based Rician noise removal for magnetic resonance imaging, IEEE Trans. Image Process. 8 (1999) 1408–1419.
[29] M.E. Alexander, R. Baumgartner, A.R. Summers, C. Windischberger, M. Klarhoefer, E. Moser, R.L. Somorjai, A wavelet-based method for improving signal-to-noise ratio and contrast in MR images, Magn. Reson. Imaging 18 (2000) 169–180.
[30] S. Zaroubi, G. Goelman, Complex denoising of MR data via wavelet analysis: application for functional MRI, Magn. Reson. Imaging 18 (2000) 59–68.
[31] J. Sijbers, A.J. den Dekker, A. Van der Linden, T.M. Verhoye, D. Van Dyck, Adaptive anisotropic noise filtering for magnitude MR data, Magn. Reson. Imaging 17 (1999) 1533–1539.
[32] G. Sapiro, D.L. Ringach, Anisotropic diffusion of multivalued images with applications to color filtering, IEEE Tram. Image Process. 5 (1996) 1582–1586.
[33] J.M. Bonny, J.P. Renou, M. Zanca, Optimal measurement of magnitude and phase from MR data, J. Magn. Reson. 113 (1996) 136–144.
[34] S. Van Huffel, H. Chen, C. Decanniere, P. Van Hecke, Algorithm for time-domain NMR data fitting based on total least squares, J. Magn. Reson. A 110 (1994) 228–237.
[35] T. Niendorf, R.M. Dijkhuizen, D.G. Norris, M. van Lookeren Campagne, K. Nicolay, Biexponential diffusion attenuation in various states of brain tissue: implications for diffusion-weighted imaging, Magn. Reson. Med. 36 (1996) 847–857.
[36] I.E. Holden, J.R. Halama, B.H. Hasegawa, The propagation of stochastic pixel ncise into magnitude and phase values in the Fourier analysis of digital images, Phys. Med. Biol. 31 (1986) 383–396.
[37] G. McGibney, M.R. Smith, An unbiased signal-to-noise ratio measure for magnetic resonance images, Med. Phys. 20 (1993) 1077–1078.
[38] A.J. Miller, P.M. Joseph, The use of power images to perform quantitative analysis on low SNR MR images, Magn. Reson. Imaging 11 (1993) 1051–1056.
[39] J. Sijbers, A.J. den Dekker, P. Scheunders, D. Van Dyck, Maximum-likelihood estimation of Rician distribution parameters, IEEE Trans. Med. Imaging 17 (1998) 357–361.